Solid-State Lasers for Coherent Communication and Remote Sensing

NASA Grant NAGW-1760

Semi-Annual Progress Report
for the period
October 1,1989 through March 31, 1990

Robert L. Byer
Principal Investigator

Edward L. Ginzton Laboratory
W.W. Hansen Laboratories of Physics
Stanford University
Stanford, California 94305

June, 1990

Solid-State Lasers for Coherent Communication and Remote Sensing

NASA Grant NAGW-1760

Robert L. Byer
Applied Physics Department
Stanford University
Stanford, California 94305

ABSTRACT

Laser development, high efficiency, high power second harmonic generation, operation of optical parametric oscillators for wavelength diversity and tunability, and studies in coherent communications are reviewed as achievements of the second semi-annual performance period of this program.

Solid-State Lasers for Coherent Communication and Remote Sensing

NASA Grant NAGW-1760

Table of Contents

Abstract ii

Table of Contents iii

Personnel Associated with the Program iv

I. Introduction 1

II. Review of Progress

A. Harmonic conversion 1

B. CW Optical Parametric Oscillator 3

C. Application of Diode Pumped Solid State Laser in Coherent Communication 6

III. Future Research 7

IV. Appendices

A. R.C. Eckardt, H. Masuda, Y.X. Fan, and R.L. Byer, "Absolute and relative nonlinear optical coefficients of KDP,KD*P, BaB_2O_4,$LiIO_3$,MgO:$LiNbO_3$, and KTP measured by phase-matched second harmonic generation," to be published in IEEE J. Quantum Electron.

B. C.D. Nabors, S.T. Yang, T. Day, and R.L. Byer,"Coherence Properties of a doubly-resonant monolithic optical parametric oscillator," *J.Opti. Soc. Am.* B, vol. 7, No.5 May 1990, pg. 815-820.

C. C.D. Nabors and R.M. Shelby,"Two-Color squeezing and Sub-Shot Noise Signal Recovery in Doubly Resonant Optical Parametric Oscillators," to be published in Phys. Rev. Letter.

D. T. Day, A.D. Farinas, and R.L.Byer, "Demonstration of a Low Bandwidth 1.06μm Optical Phase-Locked Loop for Coherent Homodyne Communication," IEEE Photonics Technology Lett., vol. 2, No. 4, April 1990, pg. 294-296.

Solid-State Lasers for Coherent Communication and Remote Sensing

NASA Grant NAGW-1760

Personnel Associated with the Program

Robert L. Byer — Principal Investigator

Robert C. Eckardt — Senior Research Associate

Martin M. Fejer — Acting Asst. Prof. of Applied Physics

Eric Gustafson — Research Associate

Charles D. Nabors — Ph.D, December 1989

Timothy Day — Graduate Student

Steven T. Yang — Graduate Student

Frank Schellenberg — Graduate Student

Solid-State Lasers for Coherent Communication and Remote Sensing

Robert L. Byer
Principal Investigator

I Introduction

NASA contract Grant NAGW-1760 supports development of solid state lasers and nonlinear frequency conversion of these sources for remote sensing and coherent optical communication applications. In the following pages, progress made during the last half year(October 1 1989 to March 31 1990) is reported. Direction for future research is also indicated.

II Review of Progress

A. Harmonic Conversion

During the last half year, emphasis has been placed on extending previous work on efficient single frequency externally resonant Second Harmonic Generation(SHG)[1] to the high power regime. Watt level coherent single frequency green radiation is ideal as a laser source for gravitational wave observatories. Other applications of the high power SHG source include the use as a pump source for coherent nonlinear optics studies, and when the 532 nm radiation is further up converted into the UV, it can be used as a light source for fine line VLSI lithography.

Previously, theoretical calculations have shown that multi-watt 532 nm radiation can be produced in an external cavity configuration with a 10 watt 1.06 μm pump using a number of different nonlinear optical crystals. These crystals include: BaB_2O_4, LiB_3O_5,

[1] W.J.Kozlovsky,C.D.Nabors and R.L.Byer,"Efficient Second Harmonic Generation of a Diode-Laser-Pumped cw Nd:YAG Laser Using Monolithic MgO:$LiNbO_3$ External Resonant Cavities," *IEEE J. Quantum Electron.* **24**, pp.913-919(June,1988).

and KTP. The more traditional $MgO:LiNbO_3$ crystal is not included due to its relatively low photorefractive damage threshold. Among the crystals examined, LiB_3O_5 appears most promising since it can be 90 degree phase matched at 1.06 μm wavelength, and it is reported to be very tolerant of high laser intensity.

In order to facilitate evaluation and comparison of the different crystals, we have opted for a discrete rather than monolithic resonator during initial trials. The enhancement resonator we have constructed has a bow tie configuration. It consists of two flat mirrors and two curved mirrors. The nonlinear crystal is placed between the two curved mirrors where a tight focal spot is located. One of the flat mirror is mounted on a piezo electric mount so that the cavity resonant frequency can be servo locked to the laser frequency. The pump source for the high power harmonic experiment is the injection locked 13 Watt Antares laser that has been previously developed in the group.[2]

So far, we have tried both KTP and BBO crystals. 532 nm radiation of 500 mw and slightly more than 1 watt has been produced using the two crystals respectively. These are less than what we expected, and the limiting factor right now is the excessive single pass power absorption of the crystals. We are currently setting up a very sensitive calorimeter for carrying out detailed crystal absorption measurements. By measuring the temperature rise in the center of the crystal, we can also tell if the absorption is due mainly to surface scattering or bulk absorption.

In addition to characterization of crystal absorption, we are also continuing the measurement of nonlinear optical coefficients of different crystals using the phase matched second harmonic technique. These measurements were carried out initially using a pulsed laser. The results of these measurements have been written up for publication. A draft of the paper is included in appendix A. At the time when the initial measurements were made, several discrepancies with previously published values were found. In addition,

[2] C.D.Nabors, A.D.Farinas, T.Day,S.T.Yang, E.K.Gustafson, and R.L.Byer,"Injection locking of a 13-watt Nd:YAG ring laser," *Opt. Lett.* **14**, 1189-1191(1989).

measurements of nonlinear coefficients of $LiIO_3$ using SHG technique and parametric fluorescence technique disagree.To corroborate the pulsed measurements, CW SHG measurements were subsequently carried out using the injection locked Antares laser. In general, the results from the CW measurements have agreed with the pulsed results. However, disagreements with parametric fluorescence measurements of $LiIO_3$ remain a puzzle. We are continuing to investigate the cause for such discrepancies.

B. Optical Parametric Oscillator(OPO)

1. Doubly Resonant OPO (DRO)

Since the demonstration of the single axial mode operation of CW Doubly Resonant OPO(DRO) in our group,[3] we have concentrated on investigating the coherence and tuning properties of CW DRO. The most significant result from the coherence studies is the confirmation that the DRO output preserves the pump coherence. The linewidth of the beatnote between the DRO signal mode and an independent single frequency Nd:GGG laser shows the same 13 KHz width as the beatnote between the Nd:YAG pump and the Nd:GGG laser, indicating that the DRO adds negligible noise to the pump. Furthermore, DRO output is found to phase locked to the pump when operated at degeneracy. Thus, at degeneracy, the DRO produces a phase coherent subharmonic of the pump. This has implication for application of the DRO as an optical frequency divider. Away from degeneracy, the phase of the signal and idler are found to be anti-correlated with each other. The results of these experiments have been published. A reprint is included as appendix B.

DRO tuning and mode control has also been studied during the last half year. Due to the requirements for simultaneous oscillation of signal and idler mode and the conservation of energy in a DRO, DRO operation is very sensitive to pump frequency

[3] C.D.Nabors, R.C.Eckardt, W.J.Kozlovsky, and R.L.Byer, "Efficient, single-axial-mode operation of a monolithic MgO:$LiNbO_3$ optical parametric oscillator," *Opti. Lett.*, **14**, 66-68(1989).

fluctuation, cavity length changes and crystal oven temperature drift. By using a stable single frequency diode pumped solid state laser as the pump and resorting to the monolithic cavity design, the effects of the first two perturbation are reduced. It is now possible to contemplate stabilized single frequency operation and continuous tuning of the DRO by changing the crystal temperature to adjust phase matching requirement, vary pump frequency to adjust energy conservation relationship, and then to tune the cavity length by applying electric field to the crystal and thus modified the simultaneous resonant conditions for signal and idler modes. To understand the control necessary to achieve slow tuning and stabilized single frequency operation of DRO, an extensive theoretical analysis has been carried out using the MgO:$LiNbO_3$ monolithic DRO as a specific example. By taking into account the temperature dependent crystal dispersion, crystal thermal expansion, the electro optic effect and the piezoelectric effect, the theory can be used to predict the tolerance required on pump frequency stability, temperature drift, and cavity length change to achieve stabilized single frequency operation and slow tuning of DRO. Initial experimental results using the MgO:$LiNbO_3$ monolithic DRO show close agreement with theory. Additional experiments are under way to demonstrate tuning and stabilized single frequency operation of DRO.

For these experiments, a novel 3:1 DRO made of congruent $LiNbO_3$ will be used. When pumped with 532 nm radiation, the 3:1 DRO will produce signal and idler wavelengths around 2 micron and 700 nm wavelengths respectively. The 2 micron regime is particularly interesting since it contains several water absorption lines. The 3:1 DRO can thus be used for remote monitoring of moisture in air. In addition, 2 micron radiation is at an eye safe wavelength and it is interesting for use for wind velocity LIDAR. Beside remote sensing and LIDAR application, the 3:1 DRO will serve as a 3 to 1 frequency divider that will be useful as part of the frequency divider chain that links the Cesium atomic clock reference to other parts of the spectrum.

2. Singly Resonant OPO (SRO)

Compared to DRO operation, SRO operation is not as highly constrained by requirement for simultaneous resonance of signal and idler. As a result, continuous tuning is much simpler in SRO than in DRO. For this and other reason, demonstration of CW SRO operation has been a long standing goal in our group. Unfortunately, previous attempts to achieve CW SRO operation were unsuccessful due to material damage limitations. Since then, we have started investigation of other suitable nonlinear optical materials for use as SRO. As our next attempt, we will investigate the transition from DRO to SRO operation by tuning the 3:1 DRO operating frequency off the mirror coating range. The pump source will be either a single line 5 Watt Ar ion laser or the 4-5 watts produced from the external resonant doubler. If the initial trial is successful, application of SRO as a tunable chirped optical radar will then be studied.

3. Squeezed State Generation

Due to its unique quantum mechanical properties, OPO has been considered a prime candidate for squeezed state generation. As part of our OPO research, we are also interested in investigating its use as a practical squeezed state generator. Applications of such squeezed state generator include ultra precise interferometric measurements such as what is required for gravitational wave detection. In addition, application of squeezed state for optical communication is also been actively pursued.

One possible way to generate "squeezed" state radiation from OPO is by taking advantage of the close correlation between signal and idler photons resulting from the parametric process. Heidmann et.al. in France has carried out an elegant experiment that demonstrates application of signal idler correlation for sub-shot noise detection.[4] In this

[4] A.Heidmann, R.J.Horowicz, S.Reynaud,E.Giacobino, and C.Fabre,"Observation of Quantum Noise Reduction on Twin Laser Beams," Phys. Rev. Lett., vol. 59,no.22, pg. 2555-2557,1987.

experiment, the signal and idler intensities are separately detected on two nominally identical detectors. Due to signal and idler correlation, the subtracted photo current from the two detectors falls below the vacuum shot noise level within the bandwidth of the OPO cavity. In their work, Type II phase matching was used which allows for separation of signal and idler modes by polarization discrimination.

In our work, we attempted to demonstrate the sub-shot noise detection by using type I phase matching in a monolithic OPO. To separate the signal and idler modes, the OPO is forced to operate very far away from degeneracy so that the wavelength difference between the two is large enough to allow separation by prisms. The best result obtained shows about 50% noise reduction of the subtracted photo currents compared to the vacuum noise level. The noise reduction is presently limited by detector efficiency, and absorption loss in the OPO crystal. The results of the squeezed state experiment has been submitted for publication. A pre-print is included in appendix C.

As a demonstration of an application for such a "Two Color squeezed" light, we injected the signal and idler beams into the two arms of a Mach Zehnder interferometer, in which one of the arm has a Pockel cell that imposes a slight amplitude modulation. We show in the experiment that sub shot noise amplitude modulation can be observed by looking at the subtracted photo currents between signal and idler. This has direct application for laser spectroscopy in detecting weak absorption lines.

C. Application of Diode Pumped Solid State Laser in Coherent Communication

The advent of diode pumped solid state laser dramatically reduced the inherent linewidth of solid state lasers. Presently, beatnote linewidth of 10 to 20 KHz can be routinely obtained. By locking to an external reference via electronic servo technique, the linewidth of these lasers can be further reduced. A beatnote linewidth of 300 mHz between two NonPlanar Ring Oscillators(NPRO) locked to a high finesse optical cavity has recently been

demonstrated in our laboratory.[5] This work was sponsored by NASA SUNLITE (NAG1-839) program. Applications of such a highly stabilized laser include gravitational wave detection, high resolution laser spectroscopy, and coherent communication.

Under the present program, we are particularly interested in exploring the application of low noise NPROs for coherent communication applications. As a laboratory demonstration of a communication link using Phase Shift Keying(PSK), an Optical Phase Lock Loop(OPLL) has been set up using two NPRO lasers serving as the transmitter and local oscillator. The details of this work are included in appendix D. By locking the phase of these two lasers at quadrature, any phase modulation imposed on the transmitter can be demodulated by looking at the error signal of OPLL. Coherent communication using homodyne PSK is the most sensitive data transmission technique. Semiconductor lasers have not been able to take advantage of extra sensitivity offered by homodyne PSK due to their inherent large phase uncertainty. Previous attempts to realize OPLL using semiconductor lasers have involved elaborate schemes for narrowing the linewidth of these lasers. Due to inherent low noise, diode pumped solid state lasers are ideal for OPLL applications. Indeed, a modest bandwidth servo loop proved sufficient to phase lock the two NPRO lasers with less than 12 mrad rms phase error. Theoretical analysis of minimal phase error in an OPLL also brings out additional advantages of diode pumped solid state lasers over semiconductor lasers in homodyne communication links. It is found that since the linewidth of a diode laser is dominated by broad band quantum noise contributions whereas the diode pumped solid state laser linewidth is low frequency flicker noise dominated, residual phase noise error of OPLL can be lower for diode pumped solid state lasers versus diode lasers with the same linewidth. This conclusion also implies that low data rate communication is feasible using diode pumped solid state lasers without incurring excessive crosstalk penalty. In our laboratory demonstration system, data rates as low as 20 KHz can be used. This is an important consideration especially for a space based

[5] T.Day, Phd. dissertation, Stanford University, 1990.

coherent communication link where data rate and laser power requirements can be traded off against each other.

III Future Research

In the next half year, investigation into coherent solid state laser sources for remote sensing and optical communication applications will continue as outlined in the original proposal. In the next quarter, emphasis will be placed on improving the conversion efficiency of discrete cavity external SHG. This will involve better characterization of crystal absorption using a calorimeter that is capable of 0.01% absorption measurement. In addition, investigation of novel nonlinear optics materials will continue as they become available.

Research in OPO will concentrate on demonstration of stabilized single frequency operation and slow controlled tuning of the 3:1 OPO. Transition into the SRO regime will also be investigated using the same 3:1 OPO by tuning off the mirror reflectivity range. Longer term research goals include demonstration of chirped optical radar using an SRO and application of the DRO for an optical frequency divider chain. Finally, more speculative research into squeeze state generation using OPOs will continue.

In the area of solid state laser development for coherent communication, the research direction will be focused on higher power, low noise, single frequency, diode pumped slab laser to serve as local oscillator in a space based coherent communication link. The laser under development for gravitational wave astronomy will satisfy all the requirements for optical communication. The proposed slab laser will be pumped by sixty 1 watt, fiber- coupled single stripe diode laser to produce 10 watts of output. The slab laser will then be injection locked to achieve single frequency operation, and stabilized to a high finesse optical cavity to reduce the linewidth further. With the progress that has been made and the planned experiments yet to be carried out, we fully expect to significantly improve solid state laser technology and nonlinear frequency conversion of these lasers for remote sensing and optical communication applications.

Absolute and relative nonlinear optical coefficients of KDP, KD*P, BaB_2O_4, $LiIO_3$, $MgO:LiNbO_3$, and KTP measured by phase-matched second harmonic generation

Robert C. Eckardt, Hisashi Masuda, Yuan Xuan Fan, and Robert L. Byer

abstract

Both absolute and relative measurements of the nonlinear optical coefficients of six nonlinear materials were measured by second harmonic generation. A single-mode, injection-seeded, Q-switched Nd:YAG laser with spatially filtered output was used to generate the 1.064 μm fundamental radiation. The following results were obtained: $d_{36}(KDP) = 0.38$ pm/V, $d_{36}(KD^*P) = 0.37$ pm/V, $|d_{22}(BaB_2O_4)| = 2.2$ pm/V, $d_{31}(LiIO_3) = -4.1$ pm/V, $d_{31}(5\%MgO:LiNbO_3) = -4.7$ pm/V, and $d_{eff}(KTP) = 3.2$ pm/V. The accuracy of these measurements is estimated to be better than 10%.

This work was supported by U. S. Army Research Office contract DAAL03-88-K-0113 and NASA Grant NAGW 1760.

R. Eckardt and R. Byer are with the Ginzton Laboratory, Stanford University, Stanford CA 94305.

H. Masuda was a visiting scientist at the Ginzton Laboratory, Stanford University, Stanford CA 94305. He is with the Sony Corporation, Corporate Research Laboratories, 1-7-4, Kohnan, Minato-ku, Tokyo 108, Japan.

Y. X. Fan is with LaserGenics, Inc., San Jose, CA 95131.

Absolute and relative nonlinear optical coefficients of KDP, KD*P, BaB_2O_4, $LiIO_3$, $MgO:LiNbO_3$, and KTP measured by phase-matched second harmonic generation

Robert C. Eckardt, Hisashi Masuda, Yuan Xuan Fan, and Robert L. Byer

I. Introduction

Careful measurements of the nonlinear optical coefficients of several nonlinear crystals of current technical interest are presented. These measurements were made by phase-matched second harmonic generation using a Q-switched Nd:YAG laser operating at 1.064 μm as the source of fundamental radiation. The laser was injection seeded to operate in a single longitudinal mode, and the output was spatially filtered to produce a Gaussian-like transverse distribution. Characterization of the pump pulse and calibration of the apparatus indicated that these measurements should be accurate to better than 10%.

This measurement was originally intended to be only a determination of the nonlinear coefficient of barium metaborate (BaB_2O_4), an interest that was motivated by observations of optical parametric oscillator thresholds that were below expected values [1]. The measurement grew to include several other nonlinear optical materials that are commonly used for second harmonic generation pumped by 1.06 μm radiation. The additional materials were measured because of a current controversy concerning the absolute magnitude of nonlinear coefficients.

Our observations use both absolute and relative measurements of nonlinear coefficients. The absolute measurements yielded values consistent with other second harmonic measurements. Measurements performed with high-power well characterized

lasers and potassium dihydrogen phosphate [2] have yielded the value d_{36}(KDP) = 0.39 pm/V, which has become accepted in the application of high-power harmonic conversion for fusion research [3]. Earlier cw measurements of 633- to 316-nm harmonic generation in ammonium dihydrogen phosphate gave a value of d_{36}(ADP) = 0.57 pm/V [4], [5]. Combining this with relative measurements between KDP and ADP yields d_{36}(KDP) = 0.41 pm/V [6]. We measured d_{36}(KDP) = 0.38 pm/V in good agreement with both earlier harmonic measurements. Values for d_{36}(KDP) determined by the technique of parametric fluorescence [7], [8] tend to be higher. Previously the value for 1.06 μm to 532 nm harmonic generation in lithium iodate $d_{31}(LiIO_3) = -7.1$ pm/V based on parametric fluorescence has been accepted as standard [9]. (No attempt was made to measure signs of the nonlinear coefficients, however when the signs are known [6] they are included.) On the parametric fluorescence $LiIO_3$ scale, the coefficient for potassium dihydrogen phosphate is d_{36}(KDP) = 0.63 pm/V for second harmonic generation pumped by 1.06 μm radiation [7]. Clearly there is a discrepancy in the accepted values for nonlinear optical coefficients.

The crystals included in the measurements reported here are KDP, $LiIO_3$, BaB_2O_4, potassium dideuterium phosphate (KD*P), potassium titanyl phosphate (KTP), and magnesium oxide doped lithium niobate (5%MgO:$LiNbO_3$). The ratio of d_{36}(KDP) to $d_{31}(LiIO_3)$ obtained in these measurements is in agreement with earlier measurements [7]. However, the value of $d_{31}(LiIO_3)$ is only 58% of the parametric fluorescence value presented in [9]. The reason for the variance is not understood. It has been suggested that the pump wavelengths may have been too close to the $LiIO_3$ absorption edge in the parametric fluorescence measurements. There has also been some question of the necessity for further corrections to deal with the birefringence of the nonlinear crystals. An anisotropic Green's function analysis [10] is discussed in the appendix with the conclusion that existing theory is appropriate for the quantitative analysis of near field second harmonic generation and parametric fluorescence.

The advantage of parametric fluorescence is that it is only necessary to measure the power ratio of the pump radiation and the generated fluorescence, whereas second harmonic requires the measurement of an absolute power and the spatial an temporal distributions of the pump field. Phase matching is also of critical importance in the second harmonic technique. Second harmonic generation, however, has the advantage that it is a direct measurement of the nonlinear coefficient under conditions that more closely duplicate actual applications. The results presented here are a study of nonlinear coefficient measurement by second harmonic generation. At this point no attempt is made to explain the nonlinear coefficient values obtained by parametric fluorescence compared to those obtained by second harmonic generation. However, clearly more work is indicated in the future regarding the nonlinear coefficient values determined by the fluorescence method.

Our second harmonic measurements were performed under near field conditions where diffraction is not of concern. Birefringent walkoff, however, was significant in the longer angle-tuned crystals. A Gaussian transverse intensity distribution was assumed, and the focused beam analysis of Boyd and Kleinman [11] was used. This cw analysis was extended to pulsed harmonic generation by numerical integration of the observed temporal distribution. Substantial effort was placed in characterizing the temporal and spatial distribution of the pump pulse. The largest single source of error in these measurements is fluctuation in spatial distribution caused by drifting of spatial filter alignment. This single error source is about equal in magnitude to all other sources of error combined.

The highest levels of harmonic conversion used here were 14%, a level at which pump depletion must be considered but can be treated adequately with a simple near field approximation. The depletion approximation was verified by observation of the dependence of harmonic conversion on pump energy in two crystals. Measurements to demonstrate that two photon absorption was not a factor were also performed in the same

crystals. In all cases phase matching tuning curves were carefully compared with calculated curves obtained from dispersion relations. The agreement of observed and theoretical tuning curves assured that the full length of the nonlinear crystal was used, and that optical distortions were not limiting harmonic conversion.

The theoretical development used to analyze our second harmonic measurements is discussed in section II. Although no new theory is presented, except for the depletion approximation, the theory is presented to make explicit the definitions that are used to describe the second harmonic generation interaction. Different factors appear in the various methods of presentation, and misinterpretation of factors abound in this field. The experimental apparatus is described in section III, and measurements are discussed in section IV. Results are summarized in section V.

II. Theory

The analysis used here draws almost entirely from earlier work [11], [12] which is reviewed in many places [6], [9], [13], [14]. MKS units are used. Definition of notation is made using a few expressions appropriate for monochromatic planewaves. The discussion continues by including the focused beam analysis and is extended to pulsed harmonic conversion by numerical integration using observed pulse shapes. A simple approximation derived empirically by calculation is used to allow for the small amount of fundamental wave depletion in the measurements. Finally a near field approximation is used to allow for an elliptical transverse beam distribution.

The electric field or electric polarization, both of which are real, can be expressed as the product of a complex amplitude and exponential summed with the complex conjugate of that product. In this format, the time dependent electric field of a monochromic planewave of angular frequency ω is

$$\boldsymbol{E}(\boldsymbol{r},t) = \frac{1}{2}\boldsymbol{E}(\boldsymbol{r},\omega)\exp\{i(\boldsymbol{k}\cdot\boldsymbol{r} - \omega t)\} + \text{c.c.}$$

The relationship between the vector components of electric polarization at the harmonic frequency 2ω resulting from the second order nonlinear interaction define the nonlinear optical coefficients $d_{jkl}(-2\omega,\omega,\omega)$

$$\mathcal{P}_i^{NL}(r, 2\omega) = \sum_{j,k=1}^{3} \varepsilon_0 \, d_{ijk}(-2\omega,\omega,\omega) E_j(r,\omega) E_k(r,\omega) \quad , \tag{1}$$

where ε_0 is the permittivity of free space. The reduced notation $d_{ijk} \rightarrow d_{im}$ allows the representation of the nonlinear optical coefficients in the customary 3 x 6 matrix. Further reduction to a single effective nonlinear coefficient d_{eff} dependent on nonlinear optical properties, phase matching, and crystal orientation is standard for modeling phase-matched second harmonic generation. With this notation the coupled equations describing harmonic generation for a monochromatic planewave propagating in the z-direction are

$$\frac{\partial}{\partial z} E(z, 2\omega) = i \kappa e^{-i\Delta k z} E^2(z, \omega) \qquad \text{and} \tag{2a}$$

$$\frac{\partial}{\partial z} E(z, \omega) = i \kappa e^{i\Delta k z} E(z, 2\omega) E^*(z, \omega) \quad , \tag{2b}$$

where $\kappa = \omega d_{eff} / (n c)$ with n the index of refraction, c the speed of light, and $\Delta k = k_{2\omega} - 2k_{\omega}$ the wavevector mismatch . Two elementary solutions to the coupled equations are

$$I_{2\omega}(l) = I_{\omega}(0)\{\Gamma l \sin(\Delta k l / 2) / (\Delta k l / 2)\}^2 \quad \text{and} \tag{3a}$$

$$I_{2\omega}(l) = I_{\omega}(0) \tanh^2(\Gamma l) \tag{3b}$$

for the respective cases of negligible pump depletion and perfect phasematching. Here $I_{2\omega}(l)$ is the harmonic intensity generated in a crystal of length l, $I_{\omega}(0)$ is the initial fundamental intensity, and $\Gamma^2 = 2\kappa^2 I_{\omega}(0) / (c\, n\, \varepsilon_0)$. Any of Equations (1), (2) or (3) can serve to define the notation used to express the nonlinear coefficients.

The dispersion in the nonlinear coefficient $d_{jkl}(-2\omega,\omega,\omega)$ is often expressed in using Miller's delta [15] δ_{jkl} and the linear susceptibilities

$$d_{ijk}(-2\omega,\omega,\omega) = \varepsilon_0 \chi_{ii}^{2\omega} \chi_{jj}^{\omega} \chi_{kk}^{\omega} \delta_{ijk}$$
$$= \varepsilon_0 \{n_i^2(2\omega) - 1\} \{n_j^2(\omega) - 1\} \{n_k^2(\omega) - 1\} \delta_{ijk} \quad . \tag{4}$$

Here $\chi_{ii}^{2\omega}$ is the linear electric susceptibility at frequency 2ω, and $n_i(2\omega)$ is the index of refraction at 2ω both for light with the electric field polarized in the direction of the i-th principal axis of the crystal. The dispersion of δ_{jkl} has been demonstrated to be small, and for experimental purposes it is usually treated as a constant.

Beam characterization measurements described in the next section show that the transverse distribution of our beam is nearly Gaussian in shape. Second harmonic conversion efficiency for cw beams with Gaussian transverse distribution in the low conversion limit is given by [11], [13]

$$\eta_{cw} = p_{2\omega} / p_{\omega} = 2\omega^2 d_{eff}^2 p_{\omega} l k \, h(B,\xi) / (\pi n^3 \varepsilon_0 c^3) \quad , \tag{5}$$

where p_{ω} and $p_{2\omega}$ are the powers of incident fundamental (after surface losses) and the output second harmonic (before surface losses), respectively. The Boyd and Kleinman focusing factor $h(B,\xi)$ is a function of the walkoff parameter B and focusing parameter ξ which are expressed by the formulas

$$B = \rho \sqrt{l k} / 2 \quad \text{and} \tag{6}$$

$$\xi = l / (k w_0^2) \quad . \tag{7}$$

Here ρ is the birefringent walkoff angle, w_0 is the 1/e amplitude radius at the beam waist, and $k = n \omega / c$ is the magnitude of the the fundamental wavevector inside the crystal.

For beam parameters used in these measurements, the approximations of $h(B,\xi)$ for the limiting case of weak focusing $\xi << 1$ are appropriate. With the added constraints of optimum phasematching, no absorption, and birefringent walkoff aperture length less than crystal length $l_a = \pi^{1/2} w_0 / \rho < l$, the focusing factor is given to the necessary accuracy by

$$h(B,\xi) \approx \xi \left(1 - t^2/12 + t^4/120 - t^6/1344 + \cdots \right) , \qquad (8)$$

where $t = 2B\,(2\xi)^{1/2}$. Since Eq. (8) assumes perfect phasematching, numerical solutions of the double integral defining $h(B,\xi)$ [11] were used to calculate phasematching curves for angle tuned crystals. Equation (8) does not include bulk material losses, however using Eq (8) and approximating bulk losses as surface losses gave the required accuracy for a 1 cm KDP crystal. None of the other crystals used had significant absorption.

The extension of equation (5) to pulsed harmonic conversion was accomplished with an integration over the observed pulse shape; $u = \int p(t)\,dt = P\,\Delta t$ where u is the total energy, $p(t)$ is the instantaneous power, P is the peak power, and Δt is an effective pulse width. Here Δt_ω and $\Delta t_{2\omega}$ were obtained by numerical integration of the observed fundamental pulse shape and the square of the observed fundamental pulse shape respectively. This treatment is applicable when the pulse has no structure or modulation on the scale picoseconds or shorter which would make group velocity walkoff important. Rewriting equation (5) for pulsed harmonic conversion

$$\eta_{calc} = \frac{u_{2\omega}}{u_\omega} = \frac{P_{2\omega}\Delta t_{2\omega}}{P_\omega \Delta t_\omega} =$$

$$2u_\omega \omega^2 d_{eff}^2 \frac{\Delta t_{2\omega}}{\Delta t_\omega^2} \frac{l\,k\,h(B,\xi)}{\pi n^3 \varepsilon_0 c^3} \quad . \qquad (9)$$

The subscript is used to indicate that η_{calc} is the conversion efficiency that is obtained from a calculation that assumes no pump depletion. Pump depletion was approximated with the relation

$$\eta_{calc} = \eta_{observed} / (1 - \eta_{observed}) \quad , \qquad (10)$$

where $\eta_{observed}$ is the observed energy conversion efficiency. Numerical integration for the near field without walkoff showed equation (10) is accurate to better than 2% for $\eta_{observed} < 50\%$.

Allowance was also made for an elliptical transverse distribution of the pump beam, a condition that existed in some of these measurements. A pump traveling in the z-direction with intensity distribution which is described by

$$I_\omega = I_0 \exp(-2x^2/w_x^2 - 2y^2/w_y^2)$$

is used. For the near field approximation, it is necessary to retain the walkoff dependance of the focusing parameter in the critical phase-matching direction which is chosen to be the x-direction. However, the beam area must be adjusted to allow for a different size in the noncritical y-direction. This is done with the substitution

$$h(B,\xi) \rightarrow (w_x/w_y)\, h(B,\xi_x)\,;\ \xi_x = l/(k\, w_x^2)\,. \tag{11}$$

When the pump depletion approximation and the allowance for elliptical transverse distribution are included, equation (9) solved for d_{eff}^2 becomes

$$d_{\text{eff}}^2 = \frac{(u_{2\omega}/u_\omega^2)}{(1 - u_{2\omega}/u_\omega)} \frac{\Delta t_\omega^2}{\Delta t_{2\omega}} \frac{w_y}{w_x} \frac{c\,\varepsilon_0\, n^2 \lambda_0^3}{16\,\pi^2 l\, h(B,\xi_x)}\,. \tag{12}$$

In Eq. (12) both $\omega = 2\pi c/\lambda_0$ and $k = 2\pi n/\lambda_0$ have been expressed in terms of the free-space wavelength λ_0 of the fundamental radiation.

The expressions for the effective nonlinear coefficients of the materials used are reproduced in Table I. The effect of nonorthogonality of the extraordinary electric field with the wavevector in the birefringent crystals is included. For negative uniaxial crystals this is done by replacing θ with $\theta + \rho$ [11] in expressions such as those given by Midwinter and Warner [16]. Here θ is the phase-matching angle and ρ is the birefringent walkoff angle. For $LiIO_3$, which has a relatively large walkoff angle, the magnitude of the value of d_{36} obtained from a measured value of d_{eff} is reduced. Indices of refraction and phasematching parameters calculated from dispersion equations are given in Table II.

III. Experimental Setup

Measurements were performed in sets that involved the comparison of two nonlinear crystals. One crystal was a well characterized reference, and the other was the crystal under test. Each set included absolute measurement of the individual crystals and a relative measurement. Phase-matching tuning curves were observed for both crystals, and surface reflections and total transmissions were measured at both fundamental and harmonic frequencies. Transverse beam characterizations were performed in the course of a measurement set, and temporal pulse shape was monitored throughout the measurements. Other calibrations and consistency checks were performed on a less regular basis.

Figure 1 shows the main components of the experimental setup which consisted of a Q-switched Nd:YAG laser, spatial filter, and two beam arrangement in which the nonlinear crystals were measured and compared. An important feature of these measurements was the use of a single-mode injection-seeded laser for the 1.064 μm pump source. Temporal properties of the laser output were determined with a 0.4 ns rise time photodiode-oscilloscope combination and a Fabry-Perot interferometer with 0.03 cm^{-1} resolution. The measurements showed that the injection-seeded laser operated in a single axial mode. We expect that the spectral distribution was near the time-bandwidth limit for the 7.0 ± 0.2 ns full-width-at-half-maximum pulse.

Pulse duration changed little over the course of these measurements. Typical oscillograms of both fundamental and harmonic pulsed are shown in Fig. 2. The leading and trailing edges of the fundamental pulse had exponential shapes with 1.4 ns time constant for the rise and 3.0 ns for the fall. Numerical integration over the measured pulse shape yielded the effective pulse width $\Delta t_\omega = 8.1 \pm 0.2$ ns and the ratio $\Delta t_{2\omega}/\Delta t_\omega = 0.67 \pm 0.02$. The ratio $\Delta t_{2\omega} / (\Delta t_\omega)^2 = 8.3 \times 10^7\ s^{-1} \pm 3\%$ was used in evaluating Eq. (12). The time response and time base calibration of the photodiode-oscilloscope combination

were checked by observing the output of a mode-locked Nd:YAG laser. The time base was accurate to within 0.6%.

Shot-to-shot energy fluctuations were caused by drifting in the alignment of the spatial filter. Figure 3a shows a histogram of individual pulse energy distribution. Most of the harmonic generation measurements consisted of averages obtained with 100 pulses. Several such averages were used in a measurement. Using 100 shot averages simplified the problem of shot-to-shot energy fluctuations and was consistent with the knife-edge transverse beam characterizations which were done with several hundred pulses. The histogram of pulse energies shows reasonable agreement with a normal distribution for which the probability of finding the fundamental energy between u_ω and $u_\omega + du_\omega$ is given by $P(u_\omega)\, du_\omega$, where

$$P(u_\omega) = \exp\{-(u_\omega - \bar{u}_\omega)^2/(2\sigma_\omega^2)\}/(\sigma_\omega\sqrt{2\pi}) \ , \tag{13}$$

$\bar{u}_\omega$ is the average fundamental energy, and σ_ω is the standard deviation. We observed $\sigma_\omega/\bar{u}_\omega = 0.08$. The standard deviation for harmonic pulses was 16%. However, the 100 shot averages reduced this value by a factor of ten. Averaging the shot-to-shot fluctuations will slightly bias harmonic measurements to higher values of harmonic power as is seen by calculating the average value of u_ω^2 given by Eq. (13)

$$\langle u_\omega^2 \rangle = (\bar{u}_\omega)^2 + \sigma_\omega^2 \ .$$

The bias was only 0.6% and was not included in the calculation.

Spatial filtering was performed by a combination of propagation into the far field, followed by aperturing the central peak of the distribution, and finally focusing through a pin hole in a vacuum spatial filter followed by recollimation. The output beam was slightly converging and reached a beam waist about 2 meters beyond the collimating lens. Beam radii were measured by a knife edge method at several positions after the collimating lens. It was demonstrated that the beam propagation closely followed that predicted for a

Gaussian distribution. Aperture and pin hole adjustment in the spatial filter provided beam waists between w_0 = 0.9 mm and 1.6 mm.

Additional checks demonstrated that there were no extraneous temporal or spectral components in the laser output. No change in beam size due to a possible second spectral component was observed with the knife edge characterization when two prisms were used in place of turning mirrors to provide a dispersion of 4 nm/mm. Photodiodes with various integrating times and sensitivities were used with different triggering and sweep rate settings of the oscilloscope, and no observable temporal components other than the Q-switched pulse were found in the laser output.

Repeated measurements of beam distribution were performed at the position where the SHG crystals were placed. The two beam arrangement allowed quick measurements of the 0.05, 0.1, 0.25, 0.5, 0.75, 0.9, and 0.95 transmission positions as the knife edge was scanned across the beam in one channel. The seven measurements were averaged to locate the center of the beam, and each of the six measurements other than the 0.5 position yielded a measurement of w_x or w_y. If the horizontal and vertical measurements agreed within experimental error they were combined to a single value w_0, and if not the beam would be treated as elliptical in shape. Figure 3b shows the beam transmittance for knife edge positions compared to values calculated for a Gaussian distribution Typical individual beam scans yielded ±3% standard deviation for waist measurements. Eight measurements made over the course of one day combined to yield a standard deviation of ±5% which was taken as the accuracy to which the beam waist was known.

The components of the two-beam arrangement were easily rearranged and interchanged for a variety of measurements. The pump beam was transmitted through a thin film polarizer and a partially transmitting mirror to provide 2 - 4 mJ of linearly polarized 1.064 μm radiation incident on the beamsplitter. Beamsplitting ratios from 50/50 to 93/7 were used. The pyroelectric energy probes used to measure pulse energy had flat spectral response and could monitor both fundamental and harmonic. Absorbing

glass filters and highly reflecting dielectric mirrors were used to eliminate fundamental radiation and transmit harmonic radiation when necessary. Calibrated neutral density filters and diffusers were used to keep measured fundamental intensities within the range of the energy probes. In addition to absolute and relative harmonic generation measurements, the apparatus also was used to measure transmissions of crystals and filters. Surface reflectivities of the crystals at both fundamental and harmonic were measured with rearrangement of components, and transmission at 532 nm was measured with the harmonic output generated in a separate crystal.

Three axes of rotational adjustment were used in the crystal mounts. Two of the axes were perpendicular to the direction of polarization and a third was parallel. A polarized alignment beam was used to determine whether the crystals were properly oriented with respect to the pump beam. A half-wave plate was used to rotate the fundamental polarization for maximum harmonic generation for measurements with type-II crystals. The angular adjustments allowed rotation through a small range of azimuthal angle to check that the crystals were properly oriented for maximum d_{eff}. All the crystals were properly oriented. However, it was necessary to use the 12 mm BaB_2O_4 crystal significantly off normal incidence to avoid problems of parallel-surface reflections.

The calibration of the two pyroelectric energy probes were intercompared, and each pyroelectric probe was compared to a thermoelectric power meter. The power meter was internally calibrated with an electrical resistance heater. The 30 Hz repetition rate of the laser allowed comparison of the average power measurement with the average pulse energy of the pyroelectric probes. The thermoelectric power meter read 3% higher than the higher of the two pyroelectric energy probes, and that probe gave reading 2% higher than the other; all agreed within 5%. The relative difference of the two probes was retained in the analysis of data, and their average reading was used as the energy calibration. The reason for this choice was that conditions were more appropriate for the pyroelectric detectors, and the 5% difference is within the expected error of all the meters

and is too small to be significant. The 5% value was taken as the accuracy of the energy measurement, which also is the accuracy stated by the manufacturer.

Energy measurement was also dependent on the accuracy of filter, attenuator, and beamsplitter calibration. Filters and attenuators were measured both in the two-beam setup described above and with a spectrophotometer. Comparison indicated accuracies of 1% in the measured transmissions. The beamsplitting ratio and probe sensitivity ratio were checked repeatedly to assure consistency in the measurements. Variations of 1/2 to 1% caused by differences in probe placement and pointing were found. Where possible critical parameters were measured with more than one method, and multiple or additional measurements were used for consistency checks and determination of accuracy.

The overall accuracy of these nonlinear coefficient measurements is estimated to be better than 10%. The average of the harmonic energy divided by the square of the fundamental energy $\langle u_{2\omega}/u_{\omega}^2 \rangle$ was determined for each series of 100 shots in making absolute measurements. A further average was made of at least five and usually more such measurements of $\langle u_{2\omega}/u_{\omega}^2 \rangle$. Typically the individual averages in one set of measurements would be consistent to ±2%. Larger variations were observed with repeated measurements that would entail recalibration, use of different samples of the same material, or different beam parameters. For example 12 measurements on three different samples of BaB_2O_4 had a ±3.6% standard deviation for the value of d_{eff}. Examination of Eq. (12), however, shows that d_{eff} can only be determined to the accuracy to which w_0 was know, and that was estimated to be 5%. The accuracy of quantities $\Delta t_{2\omega} / (\Delta t_{\omega})^2$ and $u_{2\omega} / u_{\omega}^2$ could double the uncertainty of the values of d_{eff}.

IV. Measurements

Twelve separate absolute measurements were made on three different BaB_2O_4 samples, more than used for the other materials. Also the other materials were all

measured relative to BaB_2O_4. This discussion starts with the barium metaborate measurements. The discussion is then expanded to include other materials both by absolute and relative measurement of the nonlinear coefficients.

Two of the three BaB_2O_4 samples were grown at the Stanford Center for Materials Research, and the third was grown at the Fujian Institute of Research on the Structure of Matter in the Peoples Republic of China. The Stanford Crystals were 4.1 and 11.9 mm long, and the Fujian crystal was 9.4 mm long. The tuning curves for the three BaB_2O_4 crystals agreed well with tuning curves obtained from dispersion equations and numerical evaluation of the double integral that defines the Boyd and Kleinman focusing factor $h(B,\xi)$. The calculated tuning curves were adjusted for pump depletion using Eq. (10). The observed and calculated curves for the 11.9 mm crystal are shown in Figs. 4a and b.

The effective nonlinear coefficient obtained in these measurements was $d_{eff}(BaB_2O_4)$ = 1.94±0.07 pm/V. The sign of the d_{31} coefficient relative to that of d_{22} is unknown for BaB_2O_4 , and no effort was made to determine the polarity of the crystals that were measured. Fortunately d_{31} is small compared to d_{22} ; measurements of $|d_{31}| = 0.07\ |d_{22}|$ [23] and $|d_{31}| < 0.05\ |d_{22}|$ [24] have been reported. Assuming that d_{31} is negligible, the value $|d_{22}|$ = 2.16±0.08 pm/V is obtained from the measured d_{eff}, calculated phase-matching parameters (Table I), and the appropriate definition of d_{eff} (Table II). Expressing the result with two digits as $|d_{22}|$ = 2.2 pm/V more correctly conveys the accuracy of the measurement.

Earlier measurements have placed $|d_{22}(BaB_2O_4)| = 4.1\ d_{36}(KDP)$ [23], [24]. The result of 2.2 pm/V is 37% higher than these earlier results when $d_{36}(KDP)$ = 0.39 pm/V is used. Even though $|d_{22}(BaB_2O_4)| = 5.7\ d_{36}(KDP)$ was observed here, these measurements nearly duplicated the 0.39 pm/V result for KDP.

Only a single KDP crystal was measured. The 10.4 mm long crystal was oriented for type-I phase matching, and surfaces were uncoated. The observed tuning curve again closely follows the calculated curve (Figs. 4c and d). There is a smaller amount of

birefringent walkoff in this crystal compared to the BaB_2O_4 crystal; therefore the tuning curves more closely approach the sinc-squared curve of the monochromatic planewave. Both absolute measurements of the KDP crystal and measurements relative to the 9.4 and 11.7 mm BaB_2O_4 crystals using $d_{eff}(BaB_2O_4)$ = (1.94±0.07) pm/V were closely grouped at d_{36}(KDP) = 0.376±0.005 pm/V. This small range of measurements could be coincidence, and the earlier comments about accuracy apply. More typically the combined measurements on a single material would have ±4% standard deviation. For comparison it is useful to mention that in the notation used by Craxton [2] $\{d_{36}(\text{KDP})/\varepsilon_0\}_{\text{Craxton}} = 0.78$ pm/V corresponds to d_{36}(KDP) = 0.39 pm/V in the notation used here.

In contrast to the agreement with KDP second harmonic measurements, these observations produced substantially different results compared to parametric fluorescence measurements of lithium iodate. Two $LiIO_3$ crystals 14.7 and 19.8 mm long were used for type-I second harmonic generation. These crystals were antireflection coated on input and output faces. Both crystals demonstrated good agreement between predicted and observed phase-matching curves. Birefringent walkoff was again significant as can be seen in the shape of the secondary maxima in the tuning curves of the 14.7 mm crystal. (Figs. 4e and f) Absolute measurements of the two $LiIO_3$ crystals gave $|d_{31}|$ = 4.24±0.10 pm/V, whereas measurements relative to BaB_2O_4 and KDP respectively yielded 4.02±0.19 and 4.08±0.19 pm/V. The value obtained by combining these measurements and using the known sign was $d_{31}(LiIO_3)$ = −4.1±0.2 pm/V.

Tabulations of measurements of the nonlinear coefficients of $LiIO_3$[6] show an unusually wide range of values. Of concern was that the high intensities used for pulsed harmonic generation could lower efficiency though some third order nonlinear effect such as two-photon absorption or intensity dependent refractive indices. Harmonic generation was observed as a function of fundamental pulse energy in an attempt to detect such effects. This was accomplished by attenuating the pump pulse with calibrated partially reflecting mirrors between the beamsplitter and the 19.8 mm $LiIO_3$ crystal. Figure 5a

shows the observed deviation from linearity between generated harmonic energy and square of the fundamental energy. The deviation form linearity was explained by pump pulse depletion as approximated by Eq. (10). There was no indication of reduction of harmonic generation by any third order process in this set of measurements. The four steps of attenuation gave five relative measurements of nonlinear coefficient at peak intensities ranging from 7.4 MW/cm^2 for the unattenuated pulse to approximately one-fifth that value. The five measurements had better consistency, $d_{31} = -4.13 \pm 0.05$ pm/V, than other measurements made at constant intensity.

An additional measurement was performed to test for nonlinear absorption. Fundamental energy was monitored in the reference channel, and both transmitted fundamental and generated harmonic were measured in the test channel as the 19.8 mm $LiIO_3$ crystal was tuned through phasematching. The measurement of total transmission and observed and calculated tuning curves are shown in Figs. 6a, b, and c. The measurement suggested that two-photon absorption was present but not large enough to significantly have changed the measurement of nonlinear coefficient. The second surface of the crystal was antireflection coated for 532 nm, and a 0.5% increase in total transmission was expected at peak conversion but not observed suggesting a few percent of the harmonic was lost by two-photon absorption.

Parametric fluorescence measurements have been previously performed for lithium niobate [25], [7], and it was of interest to compare second harmonic generation measurements in this material. A 6.3 mm sample of 5%MgO:$LiNbO_3$ was prepared for temperature-tuned noncritically-phase-matched second harmonic measurements. This crystal was uncoated. The previous parametric fluorescence measurements were performed with stoichiometric and congruent $LiNbO_3$ and not with the MgO doped material used for these measurements. The MgO doped $LiNbO_3$ has slightly different properties than those of the other compositions of $LiNbO_3$ but should be close enough for a useful comparison of the two techniques of nonlinear coefficient measurement.

The measured coefficient d_{31}(5%MgO:$LiNbO_3$) = - 4.7 pm/V is only 79% of the parametric florescence value for congruent $LiNbO_3$, not unreasonable agreement considering that the materials have different composition. This is supported by comparison measurements [29] of second harmonic generation by 9 mm samples of MgO doped and congruent materials under similar pumping conditions; 50.9% conversion was observed in the congruent material, and 35.2% conversion was observed in the MgO:doped material.

Two additional materials, KD*P and KTP, commonly used for 1064-nm-pumped harmonic generation were studied. Two 30 mm long KD*P crystals, one each of type-I and type-II were measured. For the type-II crystal, the result of a quantitative analysis derived from a near field calculation was used, and Kleinman symmetry was used to set $d_{36} = d_{14}$. The KD*P crystals were measured both absolutely and relative to BaB_2O_4 with the result d_{36}(KD*P) = 0.367±0.012 pm/V. This is consistent with earlier measurements relative to KDP [30], [31], [32] which yielded values in the range d_{36}(KD*P) = 0.34 to 0.48 pm/V when normalized to d_{36}(KDP) = 0.39 pm/V [3] or d_{36}(KDP) = 0.41 pm/V [6]. The tuning curves for the two KD*P crystal both indicated high quality crystals and little distortion of the pump beam. The tuning curve of the type-I crystal is shown in Figs. 4g and h.

Second harmonic generation was observed in three type-II KTP crystals. All the KTP crystals were produced by the flux growth technique in the Peoples Republic of China. The very parallel surfaces of the first two crystals produced interference which was seen in the tuning curve (Fig. 7). The third crystal was also very parallel but had a 1064 nm antireflection on one surface and a 532 nm antireflection coating on the second surface. The observed tuning curve for this crystal was in excellent agreement for rotations both about the z-axis and about an axis in the x-y plane as shown in Fig. 8. This agreement indicates a crystal of excellent optical quality, with proper orientation, and very small distortion of the pump beam. The polarization of the fundamental pulse was rotated

with a half-wave plate to produce the maximum second harmonic. The effective nonlinear optical coefficient derived from absolute harmonic measurements and measurements relative to KDP, KD*P, and BaB_2O_4 was $d_{eff}(KTP) = 3.18 \pm 0.17$ pm/V. The value calculated from earlier measurements $|d_{24}| = 7.6 \times 10^{-12}$ m/V and $|d_{15}| = 6.1$ pm/V [33] is $d_{eff}(KTP)_{calc.} = 7.3$ pm/V [22].

It is necessary to know the relative signs and relative magnitudes of d_{15} and d_{24} for the purpose of determining the size from a measurement of d_{eff}. Observation of the change in d_{eff} with crystal orientation indicates that d_{31} and d_{32} have the same sign . If it is assumed that the ratio $d_{24}/d_{15} = 1.25$ as measured previously [33], then the measured value of d_{eff} yields $|d_{24}| = 3.3$ pm/V and $|d_{15}| = 2.6$ pm/V. These values are less than half of the earlier values. The measurements, complicated by interference, made with the uncoated KTP crystals ranged from $d_{eff} = 2.1$ to 4.4 pm/V and supported the measurement of the lower value.

V. Summary

The nonlinear optical coefficient measurements reported here are summarized in Table III. These values can be taken as both relative measurements and absolute measurements. The reproducibility of the measurements was approximately ±4%. When the values are used as relative measurements, the accuracy is the same as the reproducibility. It is possible that the absolute measurements could be biased by inaccuracy in modeling and fluctuations of the transverse beam distribution, measurement of pulse shape and duration, and by the accuracy of the energy measurements. It is estimated that the accuracy of the absolute measurements of the nonlinear coefficients is ±10%.

The measurement for KDP reported here is in agreement with the nonlinear coefficient accepted for that material in high power nonlinear conversion applications, and

it agrees with the combination of relative measurements between KDP and ADP and low power cw second harmonic measurements with ADP. Furthermore the relative measurements between KD*P and KDP and between KDP and $LiIO_3$ are in agreement with earlier measurements. There is possible agreement between the absolute measurement of 5%MgO:$LiNbO_3$ and parametric fluorescence measurements of congruent $LiNbO_3$, but this is not conclusive. We have measured a significantly lower value for the nonlinear coefficients of KTP and moderately higher value for the nonlinear coefficient of BaB_2O_4 than reported in earlier measurements. Perhaps the most significant difference is the absolute measurement of the nonlinear coefficient of $LiIO_3$ which is only 58% of the value measured by parametric fluorescence.

It is remarkable, that after more than twenty-five years of study in nonlinear optics, that there should still exist such uncertainty in the scale of the nonlinear material parameters. This investigation indicates a need for further study. Performing both second harmonic and parametric fluorescence measurements on the same nonlinear crystal samples would provide useful information. The values for congruent for lithium niobate and MgO:$LiNbO_3$ will remain unresolved until this is done. The anomaly between second harmonic generation measured and parametric fluorescence measured nonlinear coefficients for lithium iodate also needs to be resolved.

It is possible to make accurate measurements of nonlinear optical coefficients using the technique of second harmonic generation provided a great deal of care is used in making the measurements and high optical quality fundamental radiation is used. The development of automatic data acquisition and reduction techniques and the availability of well characterized highly coherent lasers will make further accurate measurements tractable. The wide range of nonlinear coefficient values that have been obtained over the past twenty-five years underscores the need to use well characterized high-quality sources of fundamental radiation in nonlinear optical frequency conversion.

VI. Acknowledgements

The authors express their appreciation to the organizations and individuals who provided materials for this investigation. The barium metaborate crystals were supplied by R. Route and R. Feigelson of Stanford University and C.-T. Chen of the Fujian Institute. S. Velsko of Lawrence Livermore National Laboratory loaned the potassium dihydrogen phosphate crystal. And the magnesium oxide doped lithium niobate material was supplied by Crystal Technology, Inc. of Palo Alto CA. The authors also express their thanks to M. K. Reed who designed the spatial filter and gave valuable advice on the operation of the injection-seeded laser.

Appendix

Some detailed aspects of nonlinear frequency conversion in birefringent crystals are considered in this appendix. An anisotropic-media Green's function analysis is used to show that the treatment used here is appropriate for quantitative analysis of second harmonic generation under near field conditions. Only under tight focusing conditions will birefringence cause some astigmatism and aberration that is not already included in the analysis.

A central assumption of the Boyd and Kleinman treatment of harmonic generation by focused beams [11] is that a Gaussian harmonic beam is generated in each infinitesimal slab increment of a nonlinear crystal through which a Gaussian fundamental beam is propagated. In the case of type-I phase matching in a negative uniaxial crystal, the fundamental beam is an ordinary wave and the harmonic is extraordinary. It is further assumed that the extraordinary harmonic beam has the same focal position f and the same confocal parameter b as the fundamental beam. However, the transverse position of the extraordinary beam is displaced in a way that causes it to propagate with the appropriate

birefringent walkoff. This result was derived by Kleinman, Ashkin and Boyd [34] using an isotropic-media Green's function modified to include birefringent walkoff.

We proceed with the anisotropic-media analysis expressing results in a form similar to reference [34] to facilitate comparison. Assume that the nonlinear crystal exists between $z = 0$ and $z = l$, and is imbedded in a medium with identical linear birefringent properties but with no nonlinearity. The harmonic electric field at a point $\mathbf{r}$ is given by

$$\mathbf{E}_2(\mathbf{r},t) = \frac{\exp(-2i\,\omega t)}{4\pi\,\varepsilon_0}\int_V \exp\{-\alpha_2(z-z')/2\}\,\underset{\sim}{\gamma}\,G(\mathbf{r},\mathbf{r}')\cdot\wp^{NL}(\mathbf{r}')\,d\mathbf{r}'. \qquad (A1)$$

Here 2ω is the angular frequency of the harmonic, and α_2 is the absorption coefficient at the harmonic frequency. The Green's function $G(\mathbf{r},\mathbf{r}')$ is described later. The dyadic projection operator is defined by

$$\underset{\sim}{\gamma} = \frac{4\pi i\,\omega}{c\,n_e(\theta)}\,\hat{\mathbf{u}}\,\hat{\mathbf{u}} \quad , \qquad (A2)$$

where $n_e(\theta)$ is the extraordinary index of refraction for $\mathbf{k}_e(2\omega)$, and $\hat{\mathbf{u}}$ is a unit vector in the direction of the electric field of the extraordinary wave specified by $\mathbf{k}_e(2\omega)$. The nonlinear polarization produced by an ordinary Gaussian fundamental beam propagating in the z- direction is

$$\wp^{NL}(\mathbf{r}') = \wp_0\,\frac{\exp\{2i\,k_1 z' - \alpha_1 z'\}}{(1+i\,\tau')^2}\exp\left\{-\frac{2\,(x'^2+y'^2)}{w_0^2(1+i\,\tau')}\right\}B(z'), \qquad (A3)$$

where $\tau' = 2(z'-f)/b$ and $B(z') = 1$ for $0 \le z' \le 1$, and 0 elsewhere. The fundamental wavevector is k_1, and α_1 is the absorption coefficient of the fundamental. Everything to this point is identical with reference [34] and is presented for definition.

The Green's function used here is correct for an anisotropic dielectric [10]

$$\underset{\sim}{\gamma}\,G(\mathbf{r},\mathbf{r}') = \hat{\mathbf{u}}\,\hat{\mathbf{u}}\left(\frac{\omega}{c}\right)^2\frac{1}{k_e\sqrt{K_e}\cos\rho}\,\frac{\exp\{i\,\mathbf{k}_e\cdot(\mathbf{r}-\mathbf{r}')\}}{|\mathbf{r}-\mathbf{r}'|} \quad . \qquad (A4)$$

Equation (A4) differs from the Green's function used in reference [34] by the factor $k_e\sqrt{K_e}\cos\rho$ in the denominator, where K_e is the Gaussian curvature of the surface defined by $\mathbf{k}_e(2\omega)$, and ρ is the birefringent walkoff angle. For an isotropic medium $k_e\sqrt{K_e}\cos\rho$ is one, and the Green's functions become the same. As an example of an anisotropic material consider $LiIO_3$ oriented for phase-matched, type-I, 1064 → 532 nm second harmonic generation for which $k_e\sqrt{K_e}\cos\rho \approx 1.10$. The factor, however, cancels when the variation of k_e with direction is included in the x' and y' integration of Eq. (A1).

The paraxial expansion used to perform the integration is

$$\frac{\exp\{i\,\mathbf{k}_e\cdot(\mathbf{r}-\mathbf{r}')\}}{|\,\mathbf{r}-\mathbf{r}'\,|} = \frac{\exp\{2i\,k_1(z-z')\}}{(z-z')}\times$$

$$\exp\left\{\frac{-i\,k_1[x-x'-\rho(z-z')]^2}{2k_1\kappa_x(z-z')} - \frac{i\,k_1(y-y')^2}{2k_1\kappa_y(z-z')}\right\} . \qquad \text{(A5)}$$

Phase matching is assumed in this expression, and κ_x and κ_y are the principal curvatures of the surface defined by $\mathbf{k}_e$ (note $K_e = \kappa_x\,\kappa_y$). Again for isotropic material we would have $2k_1\kappa_x = k_e\kappa_x = 1$, and $2k_1\kappa_y = k_e\kappa_y = 1$, and Eq. (A5) would become identical with the expansion used in ref. [34].

Completing the x' and y' integrations of Eq. (A1) using (A4) and (A5) we have

$$\mathbf{E}_2(\mathbf{r}) = \underset{\sim}{\gamma}\cdot\boldsymbol{\wp}_0\frac{\exp\{2i\,k_1z-\alpha_2z/2\}}{\cos\rho}\times$$

$$\int_0^l \exp\left\{\frac{-2[x-\rho(z-z')]^2}{w_0^2(1+i\,\tau_x)} - \frac{2y^2}{w_0^2(1+i\,\tau_y)}\right\}\frac{e^{-\alpha z'}dz'}{(1+i\,\tau')} , \qquad \text{(A6)}$$

where $$\tau_x = 2\left\{z-\left[f/k_e\kappa_x-(1/k_e\kappa_x-1)z'\right]\right\}k_e\kappa_x/b \quad \text{and} \qquad \text{(A7)}$$

$$\tau_y = 2\left\{z-\left[f/k_e\kappa_y-(1/k_e\kappa_y-1)z'\right]\right\}k_e\kappa_y/b . \qquad \text{(A8)}$$

We could further manipulate the expressions (A7) and (A8) to have x-distribution and y-distribution focal positions and confocal parameters, but it is unnecessary for our purposes. We can project the solution back to the plane $z = l$, and take that as the exit surface of the

crystal. With the experimental conditions of these measurements, we are in the near field with $\tau << 1$ at this plane. In using Eq. (8) we had assumed that τ could be ignored, and the small changes in τ given by the last two equations are of no significance. In the approximation that $\tau_x \approx \tau_y \approx \tau = (z - f)/b$, equation (A6) becomes the same as Eq. (4.19) of ref. [34], the result mentioned above which leads to Eq. (2.9) of the Boyd and Kleinman focused beam analysis [11].

For parametric fluorescence in negative uniaxial crystals such as $LiIO_3$ or $LiNbO_3$, the scattered radiation or parametrically generated noise is ordinary, and an isotropic analysis of the scattering is adequate. The pump radiation used for these parametric fluorescence measurements, however, is extraordinary. Therefore it is necessary to use the angle of propagation plus the walkoff angle $(\theta + \rho)$ when calculating components of the extraordinary electric field of the pump radiation that lie in the direction of the principal axes of the crystal. In both parametric fluorescence measurements and second harmonic measurements in these crystals, the measured effective nonlinear coefficients must be converted to components of the nonlinear optical tensor using the angle $(\theta + \rho)$ [11]. For $LiNbO_3$ with $\theta = 90°$, $\rho = 0$, and there is no change from using θ instead of $(\theta + \rho)$. For $LiIO_3$ with $\theta = 30.2°$, $\rho = 4.26°$ the effective nonlinear coefficient is increased by 1.12 for a given value of d_{31} using $(\theta + \rho)$ instead of θ. This factor is not adequate to account for the discrepancy between d_{eff} measured here by SHG and previous measurements by parametric florescence.

References

1. Y. X. Fan, R. C. Eckardt, R. L. Byer, J. Nolting and R. Wallenstein, "Visible BaB_2O_4 optical parametric oscillator pumped at 355 nm by a single-axial-mode pump source," Appl. Phys. Lett. **53**, pp. 2014-2016, 1988.
2. R. S. Craxton, "High efficiency frequency tripling schemes for high-power Nd:glass lasers," IEEE J. Quantum Electron. **QE-17**, pp. 1771-1782, 1982.
3. D. Eimerl, "Electro-optic, linear, and nonlinear optical properties of KDP and its isomorphs," Ferroelectrics **72**, pp. 95-139, 1987.
4. G. E. Francois, "cw Measurement of the optical nonlinearity of ammonium dihydrogen phosphate," Phys. Rev. **143**, pp. 597-600, 1966.
5. J. E. Bjorkholm and A. E. Siegman, "Accurate cw measurement of optical second-harmonic generation in ammonium dihydrogen phosphate and calcite," Phys. Rev. **154**, pp. 851-860, 1967.
6. S. Singh, "Nonlinear optical materials," in *Handbook of Laser Science and Technology*, vol. III, M. J. Weber, Ed. Boca Raton, Florida: CRC Press, 1986, pp. 3-228.
7. M. M. Choy and R. L. Byer, "Accurate second-order susceptibility measurements of visible and infrared nonlinear materials," Phys. Rev. B **14**, pp. 1693-1706, 1976.
8. A. J. Campillo and C. L. Tang, "Spontaneous parametric scattering of light in $LiIO_3$," Appl. Phys. Lett. **16**, pp. 242-244, 1970.
9. S. K. Kurtz, J. Jerphagnon and M. M. Choy, "Nonlinear dielectric susceptibilities," in *Landolt-Bornstein, Numerical Data and Fundamental Relationships in Science and Technology, New Series, Group III, Crystals and Solid State Physics, Vol. 11*, K.-H. Hellwege and A. M. Hellwege, Eds. Berlin: Springer, 1979, pp. 671-743.
10. M. Lax and D. F. Nelson, "Light scattering in crystals with surface corrections," in *The Theory of Light Scattering in Condensed Matter*, V. N. Agranovich and J. L. Birman, Eds. New York: Plenum, 1976, pp. 371-390.

11. G. D. Boyd and D. A. Kleinman, "Parametric interactions of focused Gaussian light beams," J. Appl. Phys. **39**, pp. 3597-3639, 1968.

12. J. A. Armstrong, N. Bloembergen, J. Ducuing and P. S. Pershan, "Interaction between light waves in a nonlinear dielectric," Phys. Rev. **127**, pp.1918-1939, 1962.

13. S. K. Kurtz, "Measurement of nonlinear optical susceptibilities," in *Quantum Electronics: A Treatise, Vol. 1, Part A*, H. Rabin and C. L. Tang, Eds. New York: Academic, 1975, pp. 209-281.

14. R. L. Byer, "Parametric oscillators and nonlinear materials," in *Nonlinear Optics*, P. G. Harper and B. S. Wherrett, Eds. San Francisco: Academic, 1977, pp. 47-160.

15. R. C. Miller, "Optical second harmonic generation in piezoelectric crystals," Appl. Phys. Lett. **5**, pp. 17-19, 1964.

16. J. E. Midwinter and J. Warner, "The effects of phase matching method and of uniaxial crystal symmetry on the polar distribution of second-order non-linear optical polarization," Brit. J. Appl. Phys. **16**, pp. 1135-1142, 1965.

17. F. Zernike, Jr., "Refractive indices of ammonium dihydrogen phosphate and potassium dihydrogen phosphate between 2000 Å and 1.5 μ," J. Opt. Soc. Am. **54**, pp. 1215-1220, 1964; J. Opt. Soc. Am. **55**, pp. 210-211, 1965.

18. K. W. Kirby, C. S. Hoeffer and L. G. Deshazer, unpublished. The Sellmeier dispersion equations obtained by these authors are reproduced in reference [3].

19. K. Kato, "Second-harmonic generation to 2048 Å in β-BaB_2O_4," IEEE J. Quantum Elect. **QE-22**, pp. 1013-1014, 1986.

20. R. Herbst, unpublished. This Sellmeier equation for $LiIO_3$ is reproduced in reference [9].

21. G. J. Edwards and M. Lawrence, "A temperature-dependent dispersion equation for congruently grown lithium niobate," Opt. Quantum Electron. **16**, pp. 373-375, 1984. These dispersion equations for congruent $LiNbO_3$ were modified by changing the extraordinary coefficient A_1 from 4.5820 to 4.55207 to obtain agreement with phase-matching temperatures observed for 5%MgO:$LiNbO_3$ in harmonic and parametric generation measurements.

22. T. Y. Fan, C. E. Huang, B. Q. Hu, R. C. Eckardt, Y. X. Fan, R. L. Byer and R. S. Feigelson, "Second harmonic generation and accurate index of refraction measurements in flux-grown $KTiPO_4$," Appl. Opt. **26**, pp. 2390-2394, 1987.

23. C.-T. Chen, Y. X. Fan, R. C. Eckardt and R. L. Byer, "Recent developments in barium borate," Proc. SPIE **681**, pp. 12-19, 1986.

24. D. Eimerl, L. Davis and S. Velsko, "Optical, mechanical, and thermal properties of barium borate," J. Appl. Phys. **62**, pp. 1968-1983, 1987.

25. R. L. Byer and S. E. Harris, "Power and bandwidth of spontaneous parametric emission," Phys. Rev. **168**, pp. 1064-1068, 1968.

26. J. L. Nightingale, W. J. Silva, G. E. Reade, A. Rybicki, W. J. Kozlovsky and R. L. Byer, "Fifty percent conversion efficiency second harmonic generation in magnesium oxide doped lithium niobate," Proc. SPIE **681**, pp. 20-24, 1986.

27. D. A. Bryan, R. R. Rice, R. Gerson, H. E. Tomaschke, K. L. Sweeney and L. E. Halliburton, "Magnesium-doped lithium niobate for higher optical power applications," Opt. Eng. **24**, pp. 138-143, 1985.

28. W. J. Kozlovsky, C. D. Nabors and R. L. Byer, "Efficient second harmonic generation of a diode-laser-pumped cw Nd:YAG laser using monolithic MgO:$LiNbO_3$ external resonant cavities," IEEE J. Quantum. Electron. **24**, pp. 913-919, 1988.

29. E. O. Ammann and S. Guch, Jr., "1.06 - 0.53 μm second harmonic generation using congruent lithium niobate," Appl. Phys. Lett. **52**, pp. 1374-1376, 1988.

30. R. C. Miller, D. A. Kleinman and A. Savage, "Quantitative studies of optical harmonic generation in CdS, $BaTiO_3$, and KH_2PO_4 type crystals," Phys. Rev. Lett. **11**, pp. 146-149, 1963.

31. J. P. van der Ziel and N. Bloembergen, "Temperature dependence of optical harmonic generation in KH_2PO_4 ferroelectrics," Phys. Rev. **135**, pp. A1662-A1669, 1964.

32. V. S. Suvorov, A. S. Sonin and I. S. Rez, "Some nonlinear optical properties of crystals in the KDP group," Sov. Phys. JETP **26**, pp. 33-37, 1968.

33. F. C. Zumsteg, J. D. Bierlein and T. E. Grier, " $K_xRb_{1-x}TiOPO_4$: A new nonlinear optical material," J. Apl. Phys. **47**, pp. 4980-4985, 1976.

34. D. A. Kleinman, A. Ashkin and G. D. Boyd, "Second-harmonic generation of light by focused laser beams," Phys. Rev. **145**, pp. 338-379, 1966.

Table I. Effective Nonlinear Optical Coefficients

Crystal	Point Group	Phase-Matching	Effective Nonlinear Optical Coefficient [a]
KDP	$\bar{4}2m$	Type-I	$d_{eff} = -d_{36} \sin(\theta+\rho) \sin 2\phi$
KD*P		Type-II	$d_{eff} = (d_{14} + d_{36}) \sin(\theta+\rho) \cos(\theta+\rho) \cos 2\phi$
BaB_2O_4	3m	Type-I	$d_{eff} = d_{31} \sin(\theta+\rho) - d_{22} \cos(\theta+\rho) \sin 3\phi$
5%MgO:$LiNbO_3$			
$LiIO_3$	6	Type-I	$d_{eff} = d_{31} \sin(\theta+\rho)$
KTP[b]	mm2	Type-II	$d_{eff} \approx (d_{24} - d_{15}) \sin 2\theta \sin 2\phi - (d_{15} \sin^2\phi + d_{24} \cos^2\phi) \sin\theta$

(a) There are different conventions used for defining effective nonlinear coefficients. We choose the one in which the direction of the wavevector is specified by spherical coordinates (θ,ϕ) referenced to the crystalline axes; ρ is the birefringent walkoff angle. The positive sense of the extraordinary polarization is taken as that which has a component in the direction of the positive crystalline z-axis..

(b) The expression for KTP is an approximation that is justified by the small difference between n_x and n_y compared to the difference between n_z and n_x or n_y, and further justified because $\theta \approx 90°$ for all measurements used here.

Table II. Calculated Phase-matching Parameters

Crystal	Reference[a]	θ_{pm}	ρ	$n_o(\omega)$	$n_e(\omega)$	$n_o(2\omega)$	$n_e(2\omega)$
KDP, type-I	[17]	41.2°	1.60°	1.4942	1.4603	1.5129	1.4709
KD*P, type-I	[18]	36.6°	1.45°	1.4931	1.4582	1.5073	1.4683
KD*P, type-II		53.7°	1.42°,1.28°				
BaB_2O_4, type-I	[19]	22.8°	3.19°	1.6545	1.5392	1.6742	1.5547
$LiIO_3$, type-I	[20]	30.2°	4.26°	1.8559	1.7164	1.8975	1.7475
5%MgO:$LiNbO_3$[b], type-I	[21]	90° T = 107 C	0	2.2327	2.1527	2.3242	2.2327
KTP[c], type-II	[22]	θ = 90° ϕ = 24.3°	0.08°, 0.06°	$n_x(\omega)$ = 1.7381 $n_y(\omega)$ = 1.7458 $n_z(\omega)$ = 1.8302		$n_x(2\omega)$ = 1.7785 $n_x(2\omega)$ = 1.7892 $n_z(2\omega)$ = 1.8894	

(a) Reference is to source of dispersion equations from which parameters are calculated.

(b) $LiNbO_3$ is the only temperature tuned crystal; all the others are angle tuned at room temperature.

(c) KTP is a biaxial crystal; all the others are uniaxial.

Table III. Nonlinear Optical Coefficients

Crystal	Nonlinear optical coefficient[a] (10^{-12} m/V)	Miller's delta (10^{-2} m^2/C)
KDP	$d_{36} = 0.38$	$\delta_{36} = 2.4$
KD*P	$d_{36} = 0.37$	$\delta_{36} = 2.4$
$LiIO_3$	$d_{31} = -4.1$	$\delta_{31} = -3.8$
5%MgO:$LiNbO_3$	$d_{31} = -4.7$	$\delta_{31} = -0.84$
BaB_2O_4	$d_{eff} = 1.94$ $\|d_{22}\| = 2.2$[b]	$\|\delta_{22}\| = 4.5$
KTP	$d_{eff} = 3.18$ $\|d_{15}\| = 2.6$[c] $\|d_{24}\| = 3.3$	$\|\delta_{15}\| = 2.9$ $\|\delta_{24}\| = 3.5$

(a) Nonlinear coefficients are given for 1064 to 532 nm second harmonic generation.

(b) Assumes that $|d_{31}| << |d_{22}|$ for BaB_2O_4 [24].

(c) Using $|d_{24}| / |d_{15}| = 1.25$ [33] and assuming d_{24} and d_{15} have the same sign.

Figure captions

Fig. 1. Schematic drawing of experimental setup.

Fig. 2. Oscillograms showing fundamental (a) and second harmonic (b) pulses. The time scale for both is 2 ns/cm displayed of the horizontal axis. Vertical displacement is relative power.

Fig. 3. Measurements characterizing laser output. (a) Histogram shown fundamental pulse energy distribution. (b) Typical knife-edge measurement of transverse beam distribution and calculated transmission for a Gaussian distribution fit to the data points. Error bars were obtained using eight separate horizontal and vertical scans performed over the course of one day.

Fig. 4. Measured (data points) and calculated (solid lines) phase-matching tuning curves for different second harmonic crystals.

Fig. 5. Second harmonic generation energy conversion as a function of incident fundamental energy squared for lithium iodate (a) and lithium niobate (b) and (c). Fundamental energy was measured directly in the absolute measurement and was deduced for the harmonic generation in a reference crystal for the relative measurements. The solid lines are the calculated conversion with pump depletion, and the dotted lines without. Each data point represents a 100 shot average. The $LiIO_3$ data points which fell obviously below the others were caused by unstable mounting of the crystal.

Fig. 6. Total transmission for combined fundamental and harmonic as $LiIO_3$ (a) and $LiNbO_3$ (d) crystals are tuning through phasematching. The line drawn in the transmission measurement simply connects the data points to make them more visible. The measured phase-matching tuning curves are shown by data points and calculated tuning curves by the solid lines for $LiIO_3$ in (b) and (c) and for $LiNbO_3$ in (e) and (f).

Fig. 7. A phase-matching tuning curve for an uncoated KTP crystal which has a problem of interference of reflections from the parallel surfaces.

Fig. 8. Phase-matching tuning curves of an antireflection coated KTP crystal for noncritical rotation (a and b) and critical rotation (c and d). Data points show the observed tuning curves, and solid lines show the calculated tuning curves.

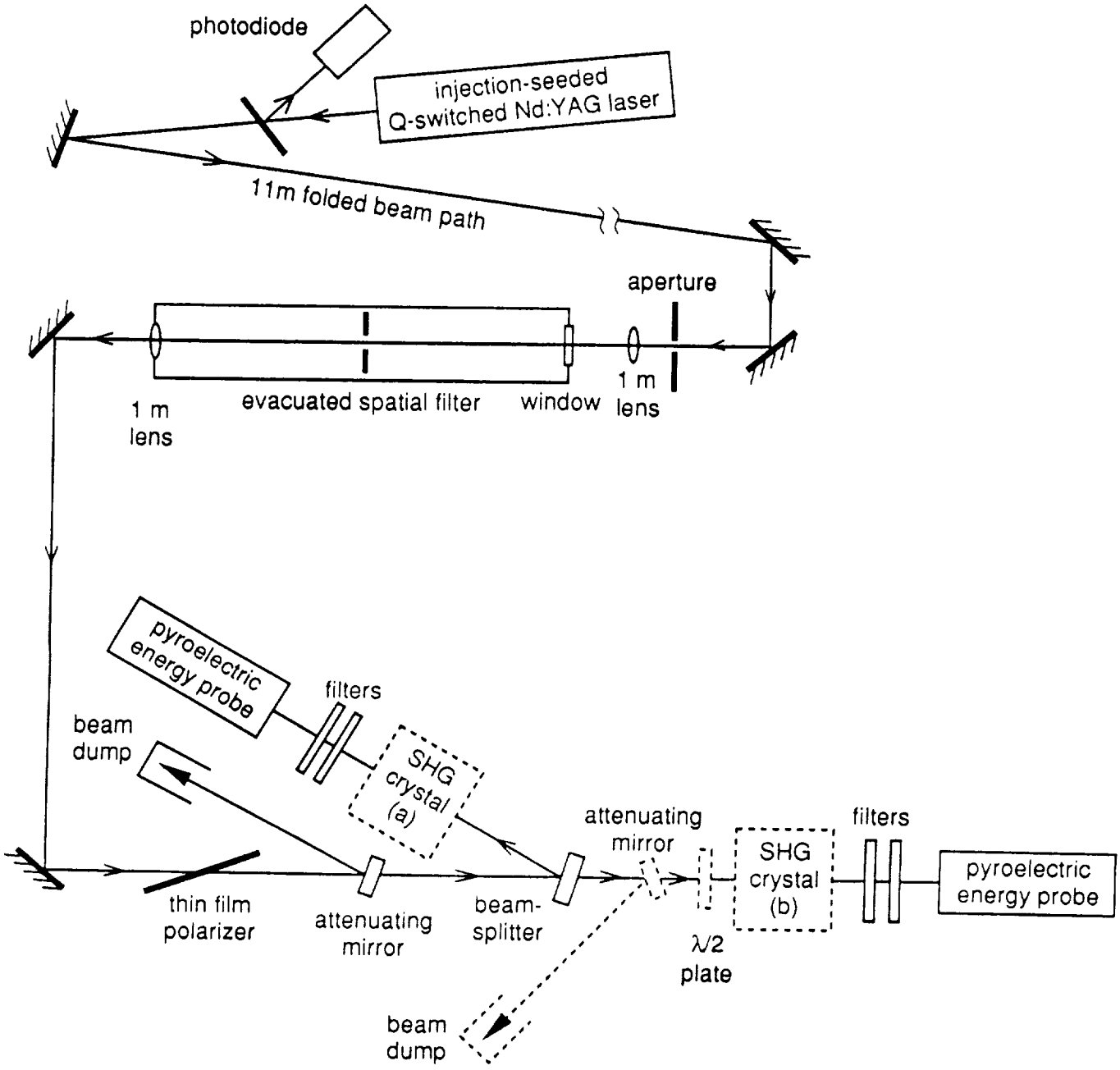
photodiode
injection-seeded
Q-switched Nd:YAG laser
11m folded beam path
aperture
1 m
lens
evacuated spatial filter
window
1 m
lens
pyroelectric
energy probe
filters
beam
dump
SHG
crystal
(a)
attenuating
mirror
filters
SHG
crystal
(b)
pyroelectric
energy probe
thin film
polarizer
attenuating
mirror
beam-
splitter
λ/2
plate
beam
dump

Figure 1

(a)

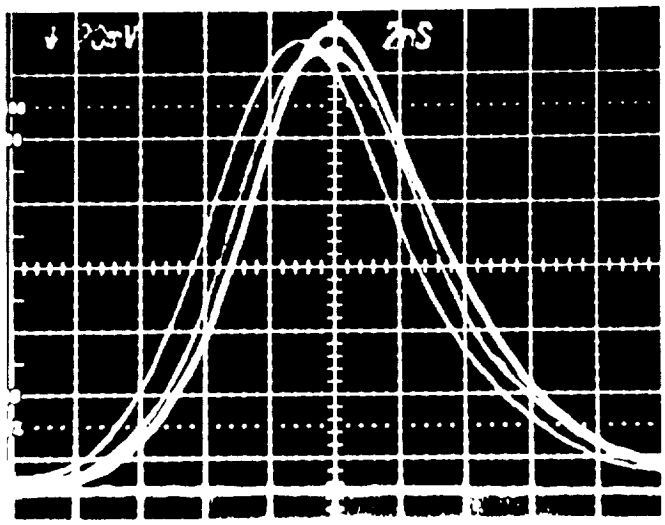

(b)

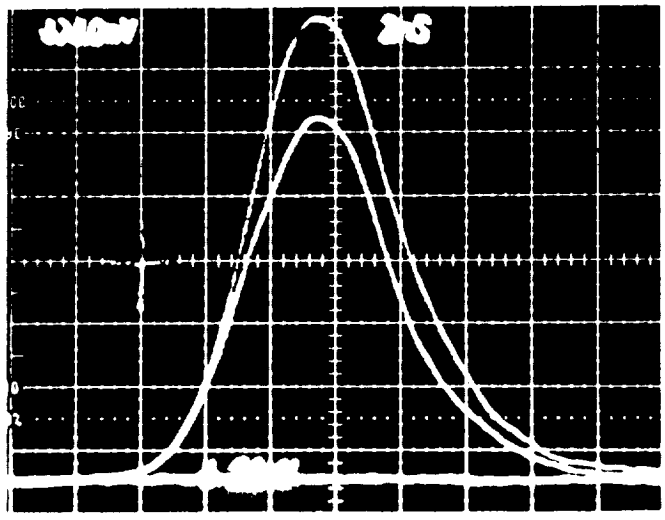

Figure 2

rev 4

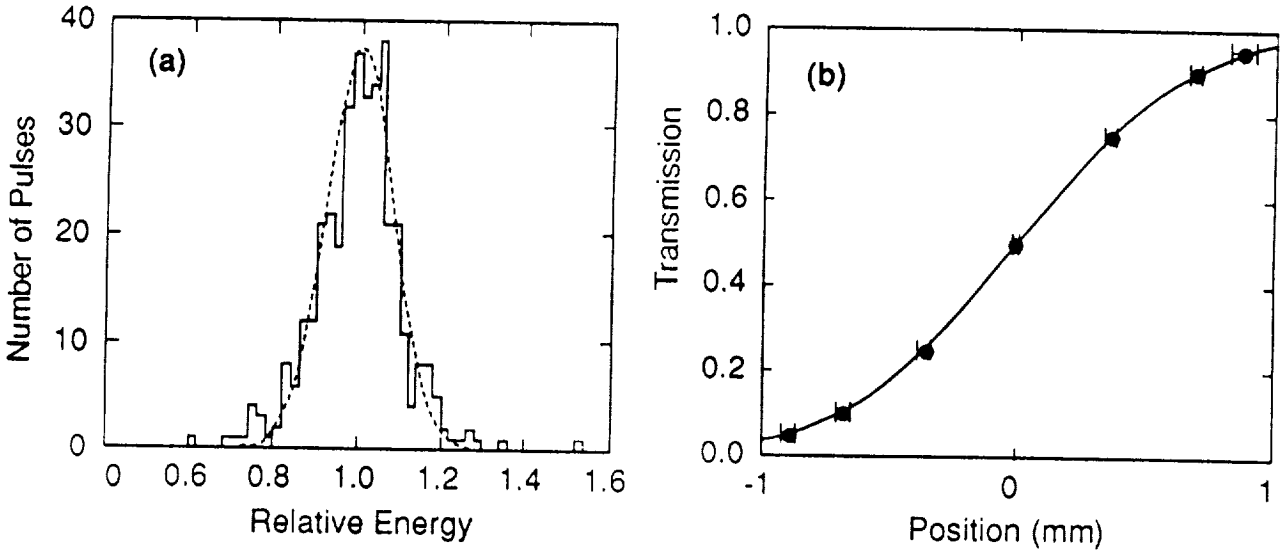

Figure 3

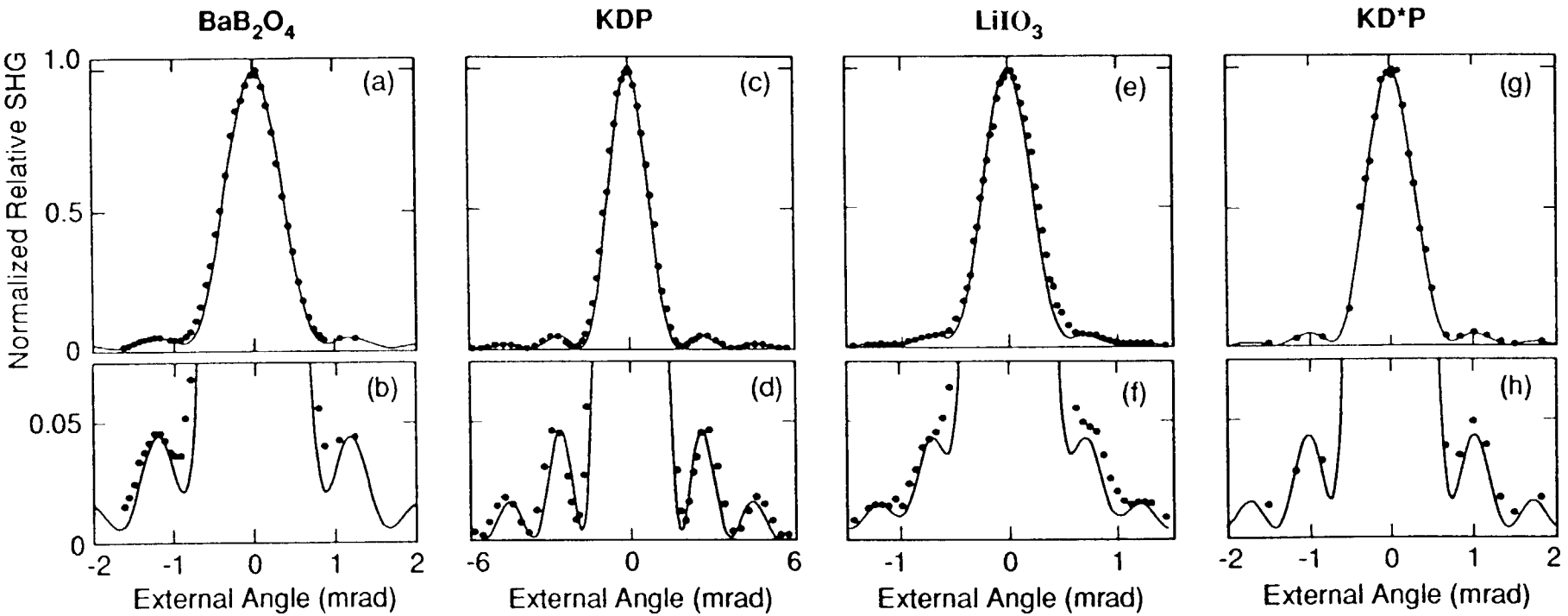
BaB2O4
KDP
LiIO3
KD*P
Normalized Relative SHG
1.0
0.5
0
0.05
0
(a)
(b)
(c)
(d)
(e)
(f)
(g)
(h)
-2
-1
0
1
2
-6
0
6
External Angle (mrad)

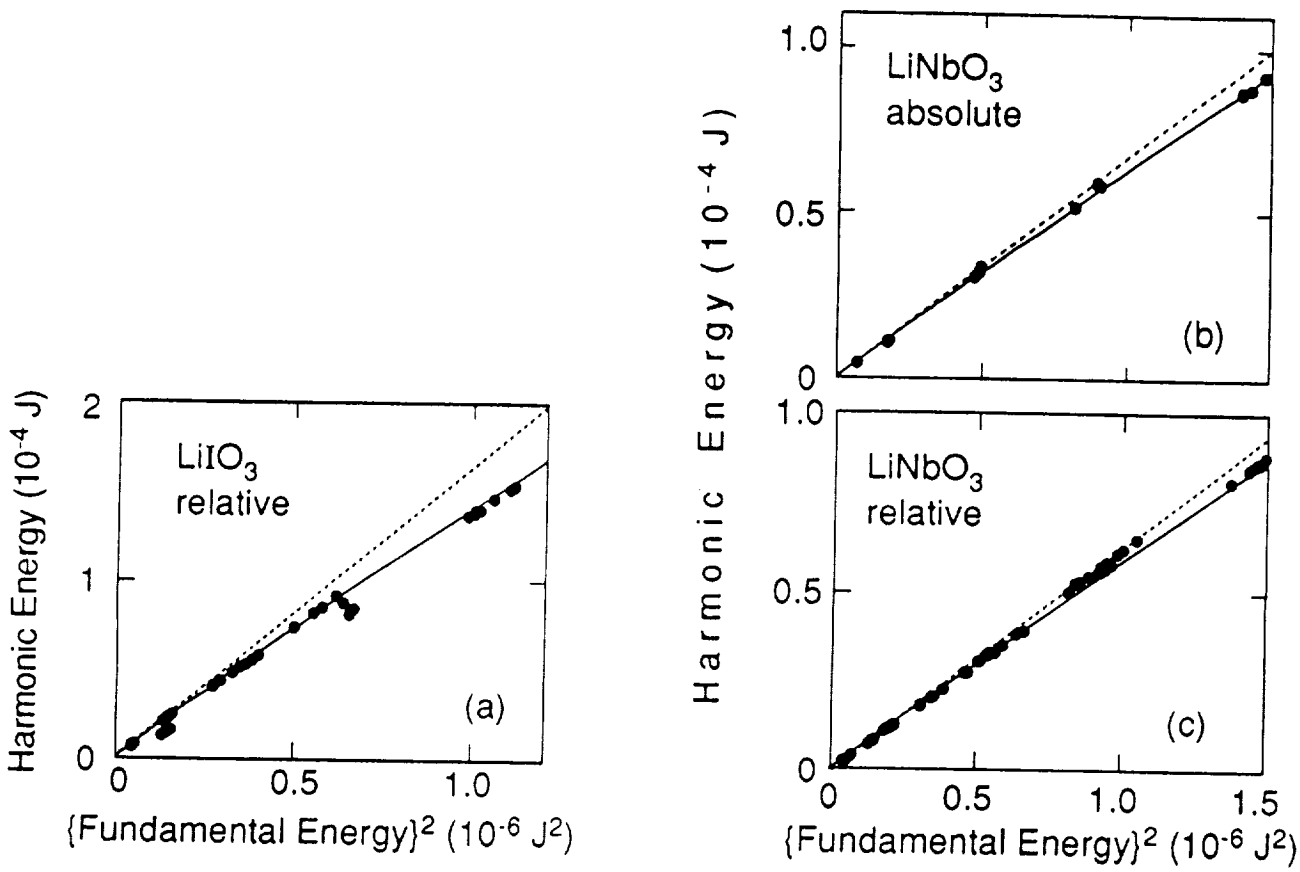
Harmonic Energy (10-4 J)
LiIO3
relative
(a)
2
1
0
0
0.5
1.0
{Fundamental Energy}2 (10-6 J2)
Harmonic Energy (10-4 J)
LiNbO3
absolute
(b)
1.0
0.5
0
LiNbO3
relative
(c)
1.0
0.5
0
0
0.5
1.0
1.5
{Fundamental Energy}2 (10-6 J2)

Figure 5

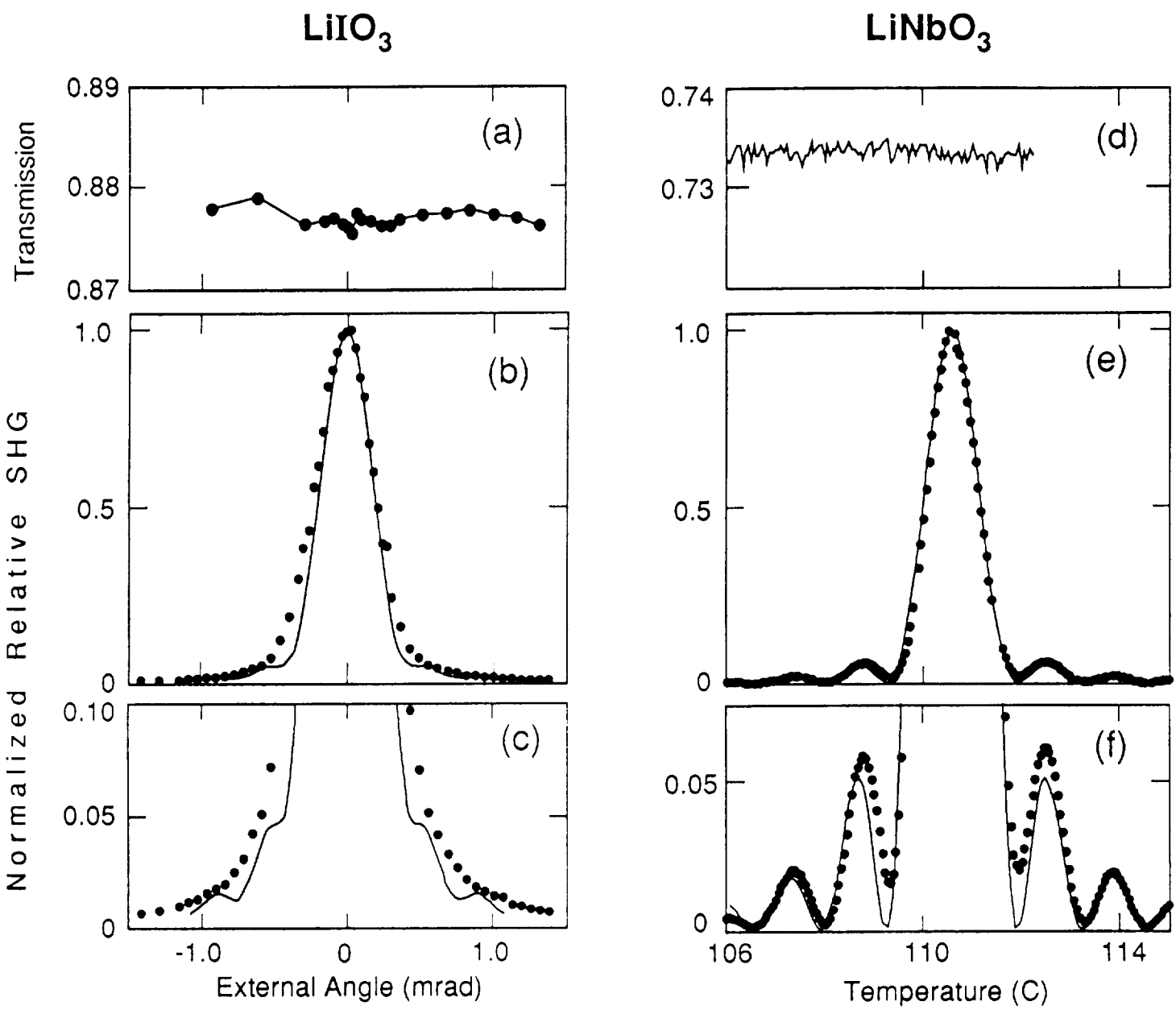
LiIO3
LiNbO3
Transmission
Normalized Relative SHG
(a)
(b)
(c)
(d)
(e)
(f)
0.89
0.88
0.87
1.0
0.5
0
0.10
0.05
0
0.74
0.73
1.0
0.5
0
0.05
0
-1.0
0
1.0
External Angle (mrad)
106
110
114
Temperature (C)

Figure 6

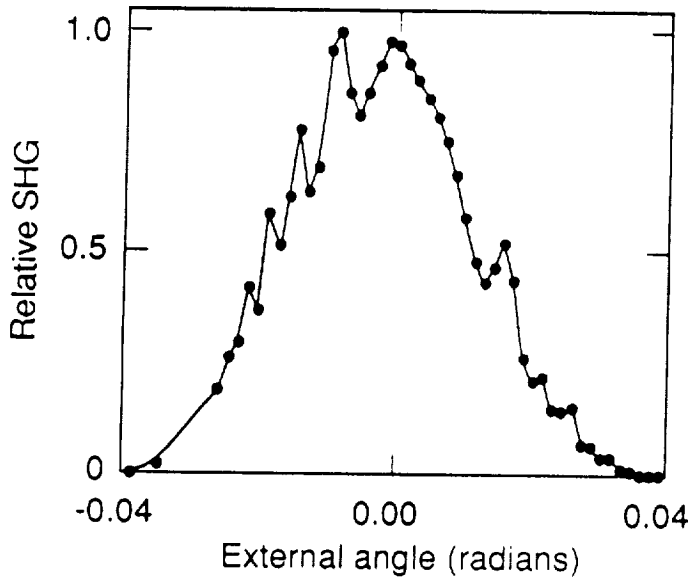

Figure 7

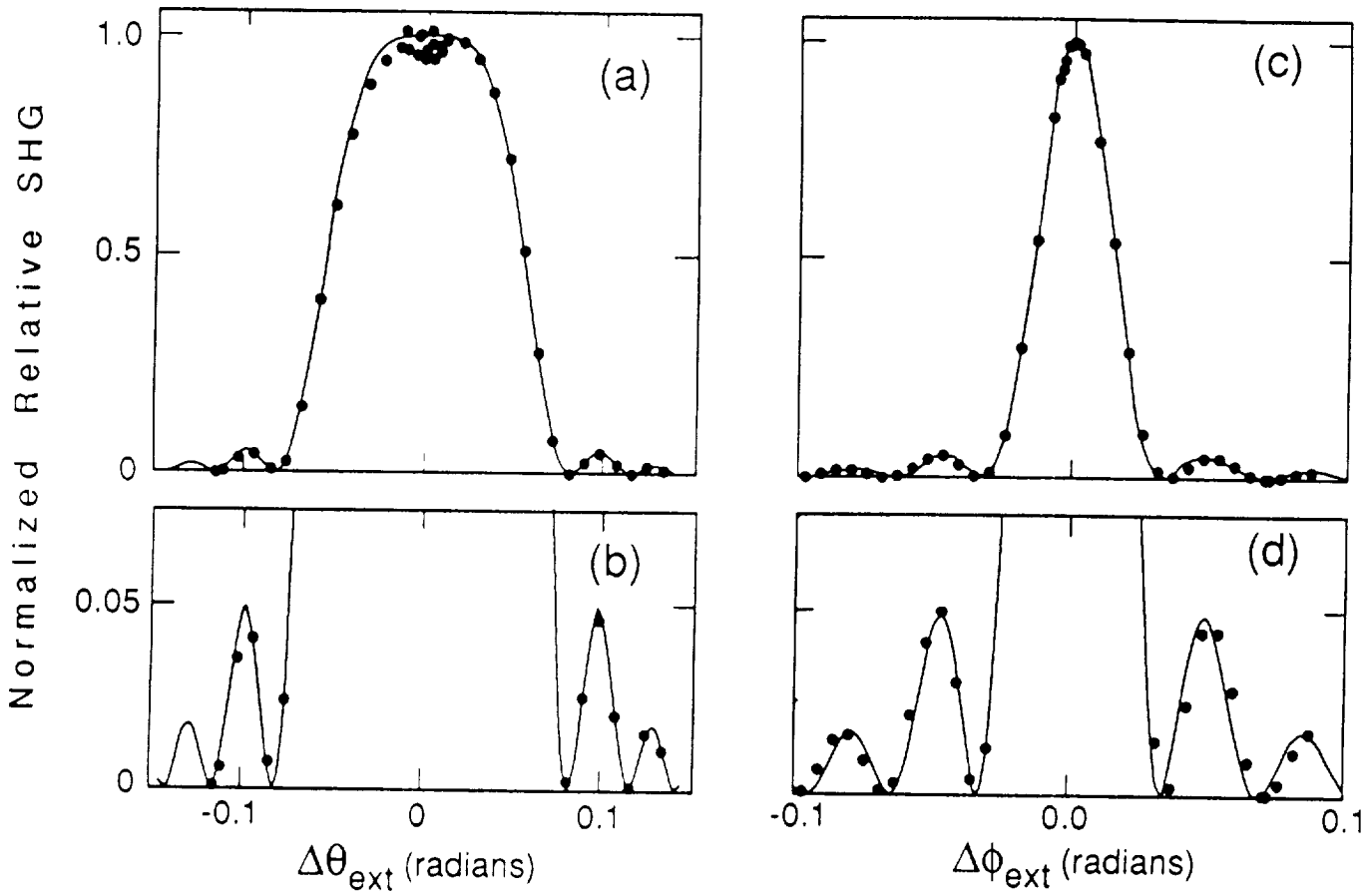
Normalized Relative SHG
1.0
0.5
0
(a)
(b)
0.05
0
-0.1
0
0.1
$\Delta\theta_{ext}$ (radians)
(c)
(d)
-0.1
0.0
0.1
$\Delta\phi_{ext}$ (radians)

Figure 2